

# Citrate–nitrate derived $\text{Sr}_{0.5}\text{Ba}_{0.5}\text{Ta}_2\text{O}_6$ tetragonal tungsten bronze nanorods: investigation of their optical and dielectric properties

Yogesh Kumar Sharma<sup>1\*</sup>, Krishna Kumar<sup>2</sup>, Chandrashekhar Sharma<sup>3</sup>, R. Nagarajan<sup>1</sup>

<sup>1</sup>Materials Chemistry Group, Department of Chemistry, University of Delhi, Delhi 110007, India

<sup>2</sup>Department of Physics and Astrophysics, University of Delhi, Delhi 110007, India

<sup>3</sup>Central Institute of Plastics Engineering and Technology, Lucknow 226 008, India

\*Corresponding author. Tel.: (+91) 09899753156; Fax: (+91) 11 2766 6605; E-mail: [yksharma@chemistry.du.ac.in](mailto:yksharma@chemistry.du.ac.in)

Received: 25 June 2011, Revised: 22 September 2011 and Accepted: 28 September 2011

## ABSTRACT

First time novel complex strontium barium tantalate,  $\text{Sr}_{0.5}\text{Ba}_{0.5}\text{Ta}_2\text{O}_6$  was successfully synthesized in 1D structure (nanorods) by citrate-nitrate gel route. Their structural properties were examined via X-ray diffractometry (XRD) and revealed the formation of tetragonal tungsten bronze (TTB) structure at as low as 1100°C. Also, FT-IR, FT-Raman, UV-vis, SEM, TEM and PL were used to identify the structure and properties of powders. Well isolated nanorods of the average diameter of ~200nm can be fabricated by this route. PL spectrum showed strong and broad visible emission band around 439nm due to particles with little surface defects. The frequency dependent dielectric dispersion of SBT50 powders sintered at 1300°C/4 h was investigated in a frequency range from 1 kHz-1MHz and at different temperatures (25°C- 450°C). It is observed that: (i) the dielectric constant ( $\epsilon'$ ) and loss tangent ( $\tan \delta$ ) are dependent on frequency, (ii) the temperature of dielectric constant maximum shift toward lower temperature side and the maximum dielectric constant ( $\epsilon$ ) was observed to be 2400 at 1 kHz. The  $T_c$  was found to be ~444-449°C and ferroelectric relaxor or diffuse phase transition like behavior was observed at around 449°C. Copyright © 2012 VBRI Press.

**Keywords:** Nanostructures; ceramics; sol-gel growth; X-ray scattering; dielectric properties.



**Yogesh Kumar Sharma** is Assistant Professor in Department of Chemistry, Swami Shradhdhanand College, University of Delhi, India. He did his Ph.D. research work at Department of Chemistry, University of Delhi. He has several research papers to his credit in International Journals of repute along with a number of publications in proceedings of national/international conferences and reviewer of few International Journals related to materials science and chemistry. He is Life time Member of Society for Materials Chemistry and Green Chemistry Network Centre (GCNC). His major research interests are use of microanalytical techniques in chemical analysis, solid state chemistry, sensing sciences, nanomaterials synthesis and their applications.



**Krishan Kumar** is Postdoctoral Fellow at University of Nice, France. He did his Ph.D. degree at Department of Physics and Astrophysics, University of Delhi and submitted his Ph.D. Thesis in 2010. He also published a number of research papers in International reputed Journals and presented his work in various national/international conferences/symposiums. He is presently working in the field of nanocrystals synthesis for optical fibers and he is expert of crystal engineering.



**Chandrashekhar Sharma** is presently working as Technical Officer-Fellow in Central Institute of plastic Engineering and Technology (CIPET), Lucknow, India. He did his Masters in Chemistry from Meerut University followed by M.Tech. (Polymer and Plastics) from Central Institute of plastic Engineering and technology (CIPET), Lucknow, India. He has published few research papers in the field of polymer nanocomposites in Journals of International repute.



**R. Nagarajan** is associate Professor in Department of Chemistry, University of Delhi. He obtained his Ph.D from Indian Institute of Science (IISc) Bangalore. He has wide experience in superconducting materials, solar cells, thin and thick films. He has presented and published more than 75 research papers in the field of materials science and technology. He did his Post Doctoral Research in various countries like France, Isri, Japan and USA. His recent research focus is on Materials Synthesis, Structure-Property relationship in solids, Laser

materials, Opto-electronic materials, Transport properties and Magnetic materials.

## Introduction

A growing interest in recent years can be seen for the synthesis of functional materials in low-dimensional nanostructures, including nanoparticles, quantum dots (zero dimension, 0 D), nanotubes, nanowires, nanorods, nanobelts (one dimension, 1 D) and nanosheets (two dimension, 2 D), because of their novel physical and chemical properties vary significantly from their bulky counterparts [1-2]. Tetragonal tungsten-bronze (TTB) ceramics, one of the most important classes next to the perovskites have been reported as functional materials and exploited for the technological applications involving large spontaneous polarization, piezoelectric, photorefractive, nonlinear optic, photocatalysis and luminescence properties in recent past [3-5]. The TTB compounds has general formula  $(A_1)_2(A_2)_4C_4[(B_1)_2(B_2)_8]O_{30}$  in which the  $A_1$  cations have 12-coordinated site,  $A_2$  cations have 15-coordinated sites, C cations have 9-fold coordinated sites and  $B_1$  or  $B_2$  cations have 6-fold coordinated sites with the space group  $P4bm$  ( $C_{4v}^2$ ) [6-7]. Jamieson *et al.* [8] and Neurgaonkar *et al.* [9] reported a detailed study on SBN, BNN and KLN for various structural revelations and exploitation for applications of TTB compounds. These materials are very promising for electroceramic applications and many researchers have shown considerable interest in the dielectric properties of such compounds. Additionally, these compounds show high Curie temperature which makes their efficiency of working at higher temperatures in transducers and detectors, their performances were found comparable to generally used perovskites such as PZT ceramics [10]. There are very few studies available on synthesis of tantalates and their various properties even these compounds show low conductivity and known for avoiding the influence of conductivity on dielectric properties as tantalum has very stable oxidation state [11]. Although, several research groups reported the synthesis of isostructural and prototype  $Sr_{0.5}Ba_{0.5}Nb_2O_6$  (SBN50) by different chemical and physical routes and their various properties earlier [12-16]. Also, a remarkable attention has been paid towards relaxors because of their noteworthy electrostrictive characteristics and very promising engineering applications [17-21]. Furthermore, Sakamoto *et al.* did complete studies on similar materials and concluded that crystallization in tungsten-bronze usually requires high crystallization temperature [22].

Recently, different preparation routes and approaches have been employed for the formation of such materials i.e. solid state, mechanochemical, coprecipitation and sol-gel etc. [23-27]. Citrate-nitrate gel approach, a simple chemical process, as it avoids the complex steps of solid state route and generates highly crystalline products with high purity, fine and narrow size distribution compared to other existing approaches [28].

In this paper, we investigate the simple and template free synthetic approach for non volatile lead-free TTB structured  $Sr_{0.5}Ba_{0.5}Ta_2O_6$  (SBT50) ceramics and obtained products were characterized for structural properties via XRD, FT-IR, Raman spectroscopy, SEM, TEM and the optical properties by UV-vis absorption and photoluminescence (PL) spectroscopy. Electrical properties were examined by impedance spectroscopy.

## Experimental

### *Materials and methods*

The citrate-nitrate gel reaction technique was employed for the synthesis of SBT50. The raw chemicals were used in the synthesis were reagent grade, barium nitrate,  $Ba(NO_3)_2 \cdot 6H_2O$  (99%, CDH), strontium nitrate,  $Sr(NO_3)_2 \cdot 6H_2O$  (99%, CDH), citric acid (99%, Thomas Baker) and tantalum (V) oxide powder (99.99%, Sigma-Aldrich). Initially,  $Ta_2O_5$  was dissolved in minimum amount of HF (40%, CDH) after heating it in water bath for 10 h. To this  $TaF_5$  solution, required quantity of  $Ba(NO_3)_2 \cdot 6H_2O$  and  $Sr(NO_3)_2 \cdot 6H_2O$  were added and mixed well. A surplus quantity of concentrated HCl was added to the above solution to dissolve the barium and strontium fluoride formed by the mixing of  $TaF_5$  and  $Ba(NO_3)_2 \cdot 6H_2O$  and  $Sr(NO_3)_2 \cdot 6H_2O$ . An Excess amount of citric acid (1:4) was added to solutions to assist complete dissolution. The solution was evaporated to dryness by heating at 100 °C on a hot plate with continuous stirring. As water evaporated, the solution became viscous and finally formed a very viscous brown gel. Increasing the temperature up to about 200 °C led to the ignition of the gel. The dried gel burnt in a self-propagating combustion manner until all gels are completely burnt out to form a loose powder. Finally, the as burnt powders were calcined at different temperatures, ranging from 500–1100°C for 12 h in air.

Thermogravimetric analysis (Perkin-Elmer Diamond TG/DTA) was performed from ambient temperature to 900 °C at a heating rate of 5 °C  $min^{-1}$  using platinum pan. The powder X-ray diffraction patterns of the samples were recorded using Rigaku Miniflex-II X-ray diffractometer employing Cu  $K\alpha_1$  radiation over the range of  $2\theta = 5^\circ-60^\circ$ . The transmission electron microscopy (TEM) images and energy dispersive X-ray analysis (EDX) measurements were performed on the Philips Tecnai  $G^2$  30 transmission electron microscope operating at an accelerating voltage of 300 kV. FT-IR spectra of the samples were gathered using Perkin-Elmer FT-IR spectrometer model 2000 employing KBr as dispersal medium. A few milligrams of the samples (roughly 10-20mg) were mixed in a mortar manually with near 50mg of KBr powder. The mixture was placed in the sample unit of FTIR equipment. Raman spectra of the samples (in compact form) were obtained using a Renishaw spectrophotometer equipped with microscope and Ar laser ( $\lambda = 514.5$  nm). Diffuse reflectance spectra of the samples were collected on Perkin-Elmer UV Vis spectrophotometer Lambda-35 attached with an integrating sphere and using  $BaSO_4$  as the reference. The photoluminescence (PL) measurements were executed using Horiba Jobin Yvon Fluoro log modular spectrofluorometer at room temperature employing CW Xenon lamp source at 310 nm. The specific area of the powders were determined by using a Micromeritics ASAP 2020 specific area and porosity analyzer using the method of Brunauer-Emmett-Teller (BET).

The calcined sample was palletized into disc using polyvinyl alcohol as binder. Finally, the discs were sintered using platinum crucible at optimized temperature 1300°C for 4 h. [29]. The bulk density of ceramics was measured by using Archimedes method by knowing the pellet weight

using a digital balance Sartorius, model BP2215, USA, in air ( $W_a$ ); weight in buoyant ( $W_b$ ) and the density of buoyant ( $\rho_b$ ). The density of the pellet was measured using the Archimedes principle i.e.  $\rho = W_a / (W_a - W_b) \rho_b$  [30]. The sample pellet (radius 4mm and average thickness 11mm) was used to record dielectric properties. The surfaces of the sintered pellet were polished and electroded with low temperature curing silver paint. The capacitance ( $C_p$ ) and loss tangent ( $D$ ) were measured as a function of frequency (1 kHz–1MHz) at different temperatures (25°C– 450°C) using a computer-controlled LCR meter (Agilent, E4980A Precision LCR Meter, USA) at chosen frequencies. The dielectric constant ( $\epsilon'$ ) was calculated from the equation,  $\epsilon' = C_p t / \epsilon_0 A$ , where  $A$  is the cross sectional area (in  $m^2$ ) of the sample and  $\epsilon_0$  is the permittivity of free space ( $8.854 \times 10^{-12} \text{ Fm}^{-1}$ ) and  $t$  is the thickness of the sample (in m). The imaginary part of the dielectric constant was calculated from the relation,  $\epsilon'' = \epsilon' \tan \delta$ , where,  $\tan \delta$  is the loss tangent.

## Results and discussion

Starting materials such as C, H, Sr, Ba and Ta could be considered as reducing elements with corresponding valences of +4, +1, +2, +2 and +5, respectively. Oxygen is as an oxidant element with valences of -2, the valence of nitrogen is considered as zero. The total computed valence of metal nitrates by mathematical summation of oxidizing and reducing valences is negative while for citric acid is positive. Consequently, the combustion can be considered as a thermally induced anionic, redox reaction of the gel wherein the citrate ion acts as reductant and nitrate ions acts as oxidant. Since the nitrate ions provide an in situ oxidizing environment for the decomposition of the organic component, slowly the rate of oxidation reaction increases. The combination of the lowering of the reaction temperature and the increase rate results in a self-propagating combustion of the citrate–nitrate gel.

### Thermal analysis

**Fig. 1** shows the TG and DTA curves and refers the change in the mass of precursor gel occurs in a wide temperature range (27–527°C) and involves three steps, the first step weight loss ~22% and one endotherm in the temperature range ~100–150°C corresponding to removal of chemically bound and sorption water from the gel. In second step the weight loss was observed to be ~25% with one endotherm between 200–300°C attributed to the decomposition of citrate-metal complex [31]. The evolution of gases such as  $\text{NO}_2$ , CO and  $\text{CO}_2$  and water vapor in large results a major weight loss. The endotherms confirm the same. Thus it helps to break up the precursor and restrict the agglomeration and turn out with the fine particles. The last third step between 300–700 °C with a weight loss of ~10% and two endotherms attributed to the crystallization of the residual organic part of the gel [32]. No further significant weight loss was observed in the temperature range above it.

### FT-IR analysis

**Fig. 2** shows comparative FT-IR spectra of the synthesized gel and the spectra of heat treated gel at different

temperatures. For the P4bm space group there should be 138 vibration modes and can be represented as

$$\Gamma^{\text{tot}} = 19A_1(z) + 15A_2 + 14B_1 + 18B_2 + 36E(x) + 36E(y)$$

where  $x$ ,  $y$  and  $z$  indicate the polarization direction of the infrared active modes [33]. The band appeared at ~3400  $\text{cm}^{-1}$  is attributed to the presence of water molecules. The band at 2367  $\text{cm}^{-1}$  corresponds to the O=C=O stretching infers the presence of  $\text{CO}_2$  in the sample after heating the organic gel. The FT-IR of the gel powders indicates a  $\text{COO}^-$  group with the vibration bands at 1418  $\text{cm}^{-1}$  (C-O) and 1589  $\text{cm}^{-1}$  (C=O) reverse symmetric stretching vibration [34]; these absorption bands remain in the further heated sample at 500°C (**Fig. 2(a)**) but suppressed at subsequent higher decomposition temperatures inferring that citrate group disintegrate with rise in temperature. The band associated with  $\text{COO}^-$  disappears due to the decomposition of organic moiety and the bands of Sr-O, Ba-O and Ta-O appears between the frequency ranges 500–800  $\text{cm}^{-1}$  and becomes dominant, the gel and heat treated samples show main bands at 500–800  $\text{cm}^{-1}$ , which are attributed to the lattice vibrations from Ta-O stretching and Ta-O-Ta bridging stretching modes [35].

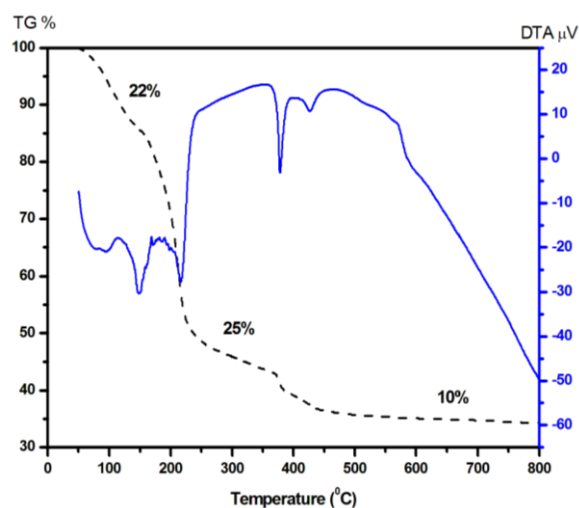
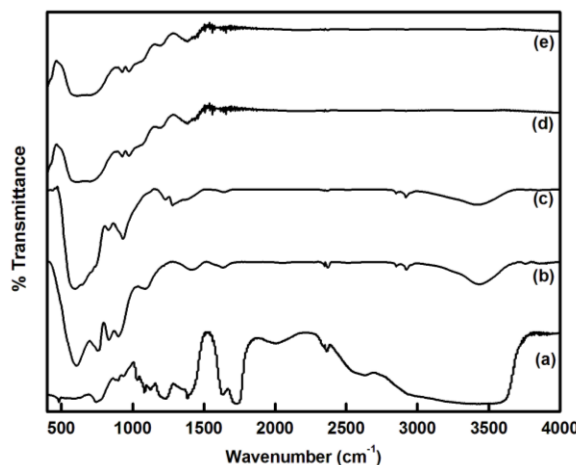


Fig. 1. TG and DTA curves of the gel.



**Fig. 2** FTIR spectra of the gel and gel treated at different temperatures (a) gel (b) 500°C (c) 700°C (d) 900°C and (e) 1100°C.

## FT-Raman analysis

To complement the FT-IR investigations, the polarized Raman spectrum of the calcined gel at 1100°C for 12 h is recorded at room temperature (Fig. 3). Assuming TaO<sub>6</sub><sup>7-</sup> anion has O<sub>h</sub> symmetry then there should be 15 vibrational modes according to 3n-6 rule, where n is the number of atoms [36]. The sample show bands at 85, 120, 175, 268, 375, 405, 475, 520, 800, 870, 908 and 961 cm<sup>-1</sup> and maintain the presence of tungsten bronze (TTB) structure of SBT50. Raman bands between 70-150 cm<sup>-1</sup> are due to the external vibration modes ν<sub>1</sub> (A<sub>1g</sub>) ν<sub>2</sub> (E<sub>g</sub>) ν<sub>3</sub> (T<sub>1u</sub>) are stretching vibration modes and ν<sub>4</sub> (T<sub>1u</sub>) ν<sub>5</sub> (T<sub>2g</sub>) and ν<sub>6</sub> (T<sub>2u</sub>) are bending vibration modes [37]. Similar to SBN50 characteristic bands i.e. Ta-O-Ta bending mode appeared at 200-300 cm<sup>-1</sup> and the symmetric stretching mode of TaO<sub>6</sub> octahedron was observed at 550-700 cm<sup>-1</sup> [38]. The absences of some of the bands are may be due to the depolarization effect, a band at around 260 cm<sup>-1</sup> is assigned to the A<sub>1</sub>(TO), other B<sub>1</sub>(TO) phonon was observed to be at 175, a very weak band at 405 cm<sup>-1</sup> is assigned to the A<sub>1</sub>(Ta-O) bond, consequently, obtained features refer to TaO<sub>6</sub><sup>7-</sup> octahedra [39].

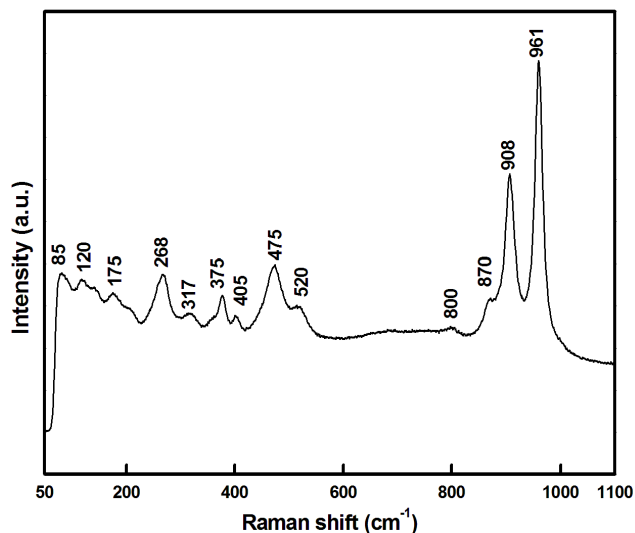


Fig. 3. Raman spectrum of the powder obtained at 1100°C.

## X-ray structural analysis

Fig. 4 shows the comparative XRD patterns of obtained gel and gel heated at elevated temperatures. The powder diffraction pattern of the obtained dried precursor gel can be seen in Fig 4(a), the pattern shows crystalline nature of the gel and  $d_{hkl}$  values were corresponded to BaF<sub>2</sub> (JCPDS:85-1342), SrF<sub>2</sub> (JCPDS: 06-0262) and TaO<sub>2</sub> (JCPDS: 19-1297). Further, powder diffraction pattern of the gel calcined at 500, 700 and 900°C are shown in Fig. 4(b) (c) and (d) respectively and established the presence of Ta<sub>2</sub>O<sub>5</sub> (JCPDS: 19-1298), SrTa<sub>2</sub>O<sub>6</sub> (JCPDS: 2 # 77-0943) and BaTa<sub>2</sub>O<sub>6</sub> (JCPDS: 74-1321) phases in the patterns. At 900°C with few secondary phases, the first emergences of the tetragonal tungsten bronze phase of Sr<sub>0.5</sub>Ba<sub>0.5</sub>Ta<sub>2</sub>O<sub>6</sub> (SBT50) which is isostructural and prototype of Sr<sub>0.5</sub>Ba<sub>0.5</sub>Nb<sub>2</sub>O<sub>6</sub> (SBN50) (JCPDS: 39-0265) was observed (Fig. 4(d)). Further calcined gel at 1100°C/12h resulted a phase pure BST50 with space group  $P4bm$  (C<sub>4v</sub><sup>2</sup>), the

calculated lattice parameters by least square fit are  $a = 12.297 \text{ \AA}$  and  $c = 3.856 \text{ \AA}$ . The particle size was calculated using Scherer's formula [40]:

$$t = K\lambda/B \cos\theta_B$$

where  $t$  is the average size of the particles, assuming particles are spherical,  $K = 0.9$ ,  $\lambda$  the wavelength of X-ray radiation,  $B$  the full width at half maximum of the diffracted peak and  $\theta_B$  the angle of diffraction. The calculated particle size is found to be ~95 nm.

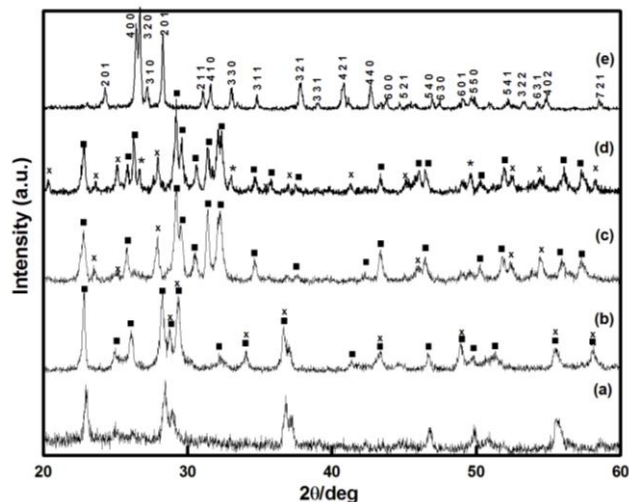
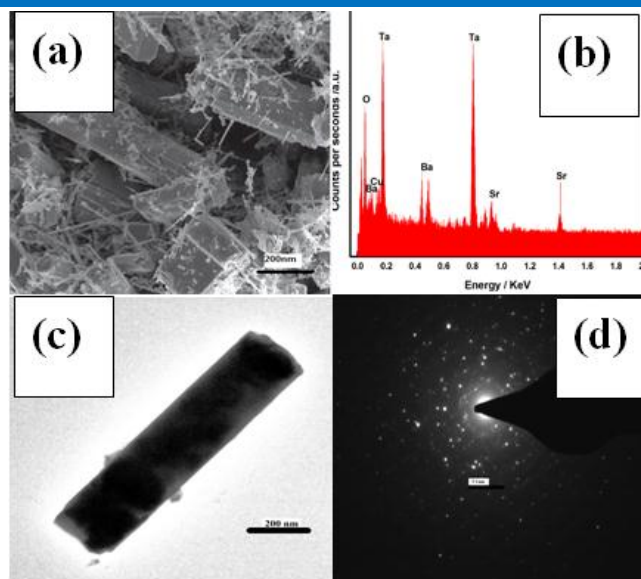


Fig. 4. XRD patterns of (a) gels and gels calcined at (b) 500°C (c) 700°C (d) 900°C and (e) 1100°C. The x denotes BaTa<sub>2</sub>O<sub>6</sub>, ■ represents SrTa<sub>2</sub>O<sub>6</sub> and \* represents SBT50.

## Composition and morphology analysis

An SEM micrograph of the SBT50 powder annealed at 1100°C reveals the microstructure exhibits rods like structures are comprised of an average diameter of ~200nm (Fig. 5(a)). It is believed that a single tetragon shaped nanorod is formed by the particles which are preferably oriented towards the tapered end of the rod. Micrographs also confirm the crystallization of rod shaped particles in tetragonal structures and the result is consistent with the XRD analysis.

EDX analysis measurements of SBT50 powders show signals from O, Ta, Ba and Sr elements, as shown in Fig. 5(b). These confirm that this material consists of essentially tantalum–oxygen–metal networks and that transition metal Sr and Ba have formed a compound with Ta. The Cu peaks are due to TEM grid. A representative transmission electron microscopy (TEM) image of the sample obtained from calcined gel at 1100°C for 12 h consisting rod like structures (Fig. 5 c). The rod have a diameter of 200 nm and a length between 400-500 nm it also confirms the established known fact that tetragonal compounds have a tendency of particle growth along c-axis [41]. Fig. 5 d illustrates the selected area diffraction pattern (SAED) of sample recorded from an area containing nanorods like structures. The prominent and clear lattice fringes are a sign of the high crystalline nature.



**Fig. 5.** (a) SEM micrograph of the powder obtained at 1100 °C (b) EDAX spectrum of the powder obtained at 1100°C (c)Transmission electron micrograph of powder obtained at 1100°C and (d) SAED spectrum of the powder obtained at 1100°C.

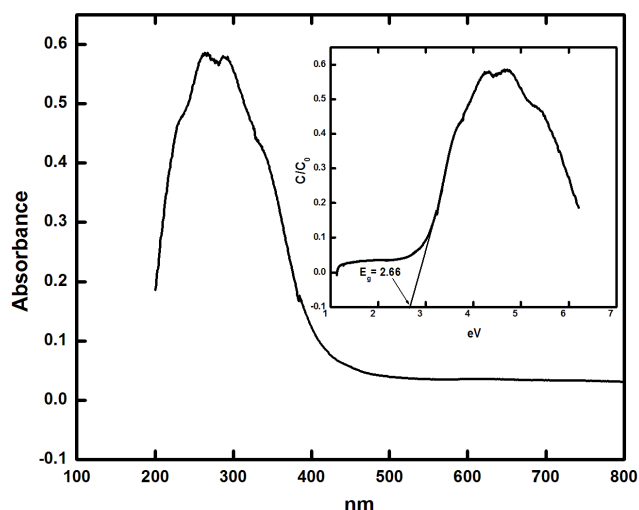


**Fig. 6.** Diffuse reflectance spectrum of the powder obtained at 1100°C, the calculated band gap using Kubelka-Munk function (inset).

#### UV-vis and photoluminescence (PL) analysis

The UV-vis diffuse reflectance experiment is done to examine the visible light response of sample obtained through gel calcined at 1100°C. The diffuse reflectance (DR) UV-vis spectrum of nanorods show a broad UV-visible light absorption band in the region 200-500 nm (**Fig. 6**). The band gap absorption edge of the prepared nanorod is determined to be 446 nm. The estimated value of the indirect band gap, calculated using Kubelka-Munk function by extrapolating the linear portion of the graph to the x-axis is 2.66 eV (inset of **Fig. 6**). The  $E_{\text{gap}}$  value (2.66 eV) suggesting the presence of intermediary energy levels within the band gap. In this case, these energy levels are arising from the structural order–disorder at long and short-range, this type of broadband visible luminescence was also observed in various perovskite titanates whose particle size was in nanometre scale [42].

**Fig. 7** illustrates the comparative photoluminescence emission (PL) spectrum of heat treated gel at 500, 700, 900 and 1100°C for 12 h. The gel did not show any significant emission band while the heat treated samples show the broad emissions at 416 nm and 439 nm, which show that there must exist certain localized levels within the forbidden gap because the direct electron transition between the valence band and the conduction band should not be allowed. This kind of luminescence occurs due to the recombination of an electron in the conduction band with a hole in the valence band, producing a band-to-band transition; the slabs are made up of  $\text{TaO}_6$  octahedra connected by sharing corners. Blasse *et al.* [43] reported PL of niobates containing oxygenous octahedra and metal cations,  $\text{Sr}^{2+}$ ,  $\text{Ba}^{2+}$  excited by light at the absorption edge region from 350 nm to 500 nm and concluded that luminescence is due to a radiative transition from an excited state to the ground state within the  $\text{TaO}_6^{2-}$  complex. Since  $\text{Sr}^{2+}$ ,  $\text{Ba}^{2+}$ , and  $\text{Nb}^{5+}$  ions have electron configurations of  $(4s^24p^6)$ ,  $(5s^25p^6)$ , and  $(4s^24p^6)$ , respectively. Here the outermost electrons are  $p$  electrons, these transitions are caused by crystal field splitting of the multiplets of  $\text{Sr}^{2+}$ ,  $\text{Ba}^{2+}$ , and  $\text{Ta}^{5+}$ . These transitions may be related to the transition between the  $\text{Ta}^{4+}$  polaron state and the valence band as has been observed in case of SBN [44].

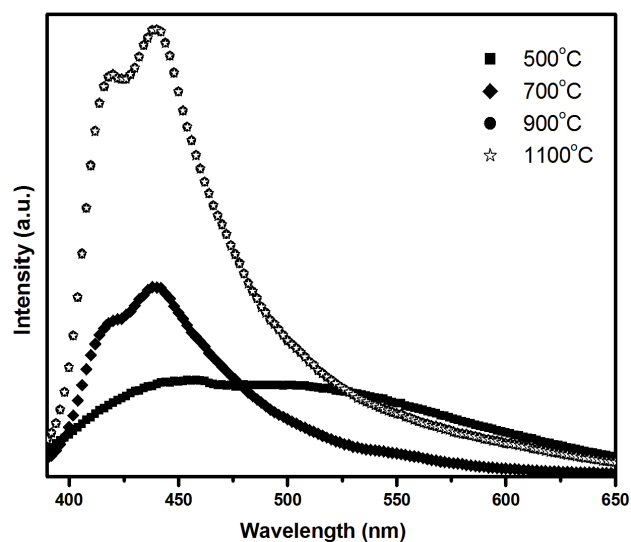


**Fig. 7:** PL spectra of (a) gel and gel calcined at (b) 500°C (c) 700°C (d) 900°C and (e) 1100°C.

Under excitation, the electrons are excited from the most filled molecular orbitals localized at  $\text{O}^{2-}$  ions from the valence band, to one of the least filled molecular orbitals localized mainly at  $\text{Ta}^{5+}$  ions in the conduction band. The transition from the excited  $\text{TaO}_6^{2-}$  complex to the ground state is accompanied by a luminescence, which proves to be structurally sensitive. Srivastava *et al.* explained that the excitation and emission maxima of the tantalates are always at energies higher than those of the corresponding niobates due to the higher 5<sup>th</sup> ionization potential of tantalum as compared with niobium [45]. Wachtel investigated the self-activated luminescence of  $\text{M}^{2+}$  niobates and tantalates in the 60's [46]. In tantalates, the excitation is due to the transfer of an electron from one of the highest filled molecular orbitals on adjacent oxygen ( $\text{O}^{2-}$ ) to one of the lowest unfilled orbitals located on the  $\text{Ta}^{5+}$  ion, likewise as

in  $\text{Nb}^{5+}$ . The alkaline earth metals and its delocalized p electrons might be able to participate in the  $\text{O}^{2-}$  to  $\text{Ta}^{5+}$  charge transfer, which would enhance the luminescence intensity. This class of phosphors is known as “self-activated” because the host lattice both absorbs and emits the radiation. Tantalum has approximately the same electronegativity as Nb and it is expected to show similar behaviour in alloy system. In SBT50 the electrons are promoted from  $\text{O}^{2-}$  bonding orbitals in the ground state, to the  $\text{Ta}^{5+}$  antibonding orbitals in the excited state, consequently the spectral bands are broad. It is well known that while the components of a continuous solid solution have the same crystal structure, the compositional changes cause a change in the lattice parameter, which leads to an expansion or a contraction of the lattice. The electron-phonon interaction can be explained on the basis of difference between the excitation energy and the emission maximum [47]. The presence of emission only in sample calcined at high temperature might be due to the formation of a small polaron by the photon absorption and the self trapped excitons (STE) formation by the intrinsic surface states and result defects and thus photon emission takes place. The gel powder which is having agglomerated particles, it seems quite impractical to see STE luminescence at temperatures lower than  $400^\circ\text{C}$  due to its weak binding energy and short radiative lifetime. Photoluminescence spectra of the product depend not only on the nature of product but also on shape and size [48]. This is the first report on photoluminescence behaviour of 1D shape SBT50, the band gap calculated using UV-vis absorption spectra and photoluminescence spectra are almost same and indicate that the product is highly crystalline as direct and indirect band gaps are equal which is possible only when the synthesized product have no impurity and have very good crystallinity.

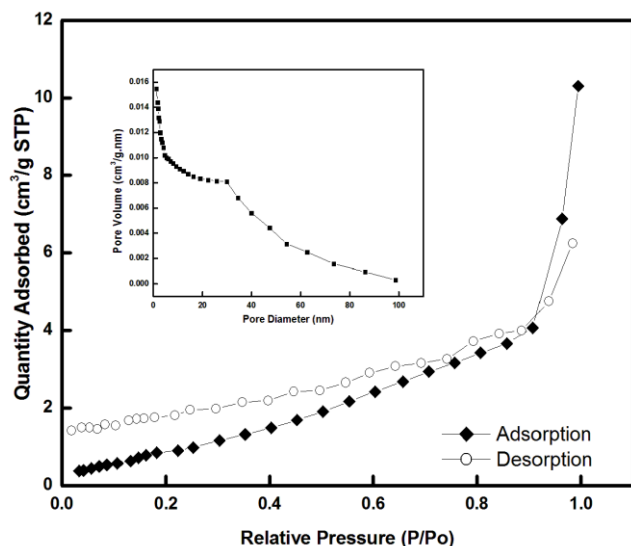


**Fig. 8.**  $\text{N}_2$  adsorption/desorption isotherm and the corresponding pore size distribution (Inset) of the as prepared SBT50 nanorods.

#### Physisorption analysis

**Fig. 8** shows the  $\text{N}_2$  adsorption desorption isotherm. The measurement showed that the BET surface area was  $3.66$

$\text{m}^2/\text{g}$  and the pore size located around  $15.31\text{ nm}$  (inset of **Fig. 8**). According to the TEM image the surface area should be more, the present values of BET surface area might be due to the coalescence of SBT50 powder during the measurement or due to large density [49]. In general, the adsorption and desorption of gas molecules on the surface of catalyst related to the catalytic properties of that material. The high pore volume containing compounds always has more unsaturated surface coordination sites and these sites enhance the properties through providing surface to sites.

The sintered density of the sample determined experimentally by the Archimedes method was found to be above 92%.

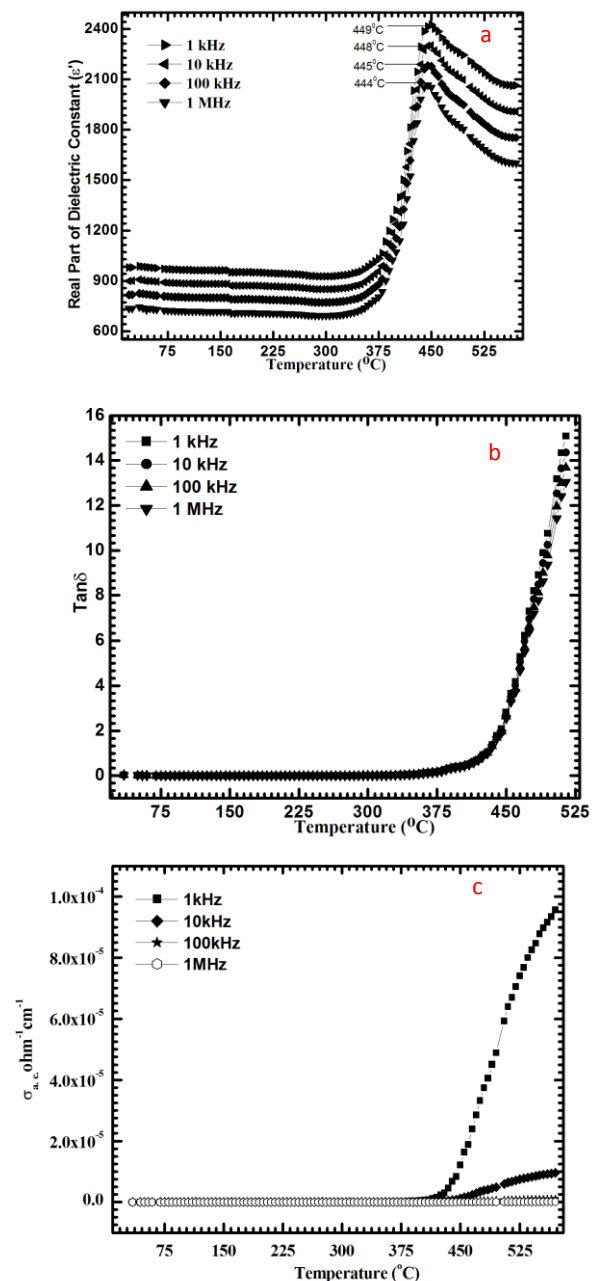


**Fig. 9** (a). Variation of real part of dielectric constant with temperature at different chosen frequencies of the sample pellet sintered at  $1300^\circ\text{C}/4\text{h}$ . (b): Variation of dielectric loss with temperature at different chosen frequencies of the sample pellet sintered at  $1300^\circ\text{C}/4\text{h}$ . (c): Variation of a. c. conductivity with temperature at different chosen frequencies of the sample pellet sintered at  $1300^\circ\text{C}/4\text{h}$ .

### Electrical and dielectric analysis

**Fig. 9** shows the dielectric characteristics of samples as functions of temperature and frequency. **Fig. 9 a** illustrates the result obtained for real part of dielectric constant ( $\epsilon'$ ) as a function of temperature at different frequencies. When the real part of the dielectric constant ( $\epsilon'$ ) was plotted against the temperature, the permittivity at 1 kHz underwent a transition at 449°C which is the transition from ferroelectric to paraelectric state (Curie temperature,  $T_c$ ).

The maximum dielectric constant ( $T_m$ ) of approximately 2400 was observed at 449°C at 1 kHz. The high value of  $\epsilon'$  observed at low frequency might arise from different types of polarization viz., electronic, dipolar, interfacial and ionic orientation etc [50]. The dielectric constant showed frequency dependence below the phase transition temperature increased. This phenomenon is called as ferroelectric relaxor behaviour. In addition, The  $T_m$  (phase transition temperature) shift towards higher temperature at low frequency confirms diffuse phase transition behavior or relaxor behaviour which is quite similar to SBN50 [51]. The dispersive behavior of the dielectric constant could also be due to disorders in atomic arrangements because the  $Sr^{2+}$  and  $Ba^{2+}$  and vacancies at site A are randomly distributed and (i) polarized structure of SBT50 and (ii) associated mobility of the charge carriers [52]; for SBT50 we can assume local and macroscopic polarization states, the two possible local states separated by energy barrier. At high temperatures these barriers can be overcome due to thermal energy, but at lower temperatures activation barrier is comparable to thermal energy and thus allow relaxation process by changing in polarization states. It also resembles the results observed in tungsten bronze SBN crystal [53]. The variation of imaginary part of dielectric constant ( $\epsilon''$ ) with temperature at chosen frequencies was also studied. The values of the  $\epsilon''$  were almost in the same range up to 420 °C with applied frequencies below 1 kHz. After 420°C, a jump in the  $\epsilon''$  was observed with increase in temperature at 1 kHz. The maximum  $\epsilon''$  observed was 2500 at 573 °C. The variation of the  $\epsilon''$  with increasing frequencies at chosen temperatures followed a trend similar to the real part of the dielectric constant.

The variation of dielectric loss tangent ( $\tan\delta$ ) as a function of temperature at different frequencies is shown in **Fig. 9 b**. The high values of  $\tan\delta$  or in other words high ionic conductivity associated with BST50 at  $T_c$  suggests that there could be a coupling between space charge and ferroelectricity [54]. The loss tangent  $\tan\delta$  peaks were observed at higher temperatures ( $\geq 375^\circ\text{C}$ ) which shift towards the higher frequency region (with rise in temperature). The temperature versus  $\epsilon'$  and loss tangent  $\tan\delta$  shows that at higher frequency of the order of 1 MHz, the loss is minimum that infers that SBT50 ceramics can be used in high magnitude frequency devices.

**Fig. 9 c** shows the a.c. conductivity ( $\sigma_{ac}$ ) of BST50 as a function of temperature. The conductivity ( $\sigma_{ac}$ ) increased with increase in temperature at lower frequencies and this trend was not observed at higher frequencies. The increasing trend of  $\sigma_{ac}$  in the low frequency range may be due to the disordering of cations between the adjacent sites. It was observed that at all the chosen frequencies,  $\sigma_{ac}$  remained constant from 30°C to 410°C and highest conductivity ( $9 \times 10^{-5} \Omega^{-1}\text{cm}^{-1}$ ) was observed at  $\sim 572^\circ\text{C}$ ,

thereafter decreased to some extent. Such a behavior is very typical of disordered materials [55]. It was observed that clearly defined peaks of conductivity were observed at 1 kHz, 10 kHz and therefore an almost flat behaviour was observed at 100 kHz and 1 MHz. The effects of morphology and the substitution with sodium, potassium, lithium and the Sr/Ba ratio on the properties of SBT50 are now under investigation.

### Conclusion

In summary, a facile citrate-nitrate gel approach was adopted for  $Sr_{0.5}Ba_{0.5}Ta_2O_6$  (SBT50) ceramics and the obtained powders consist fine nanorods like morphology. The resulting SBT50 was found to be isostructural to  $Sr_{0.5}Ba_{0.5}Nb_2O_6$  (SBN50) and the compound has a fairly good lattice match. SBT50 crystallizes in a tetragonal structure belonging to the  $P4bm$  ( $C_{2v}^2$ ) space group, where Ta cations have six-fold coordination originating two families of  $TaO_6$  octahedra, which occupy sites with  $C_{2v}$  and  $C_1$  symmetry, respectively. The optical and dielectric properties of the prepared SBT50 are also reported; the values of dielectric constant were in the range comparable to the reported SBN50 and found the maximum values approximately 2400 at 449°C and 1 kHz. The highest conductivity ( $9 \times 10^{-5} \Omega^{-1}\text{cm}^{-1}$ ) was observed at  $\sim 572^\circ\text{C}$  and synthesized ceramics exhibited the characteristic behaviour of relaxor dielectrics. Since the synthesis route adopted in the present work is economically more viable, large scale production of this kind of 1D superstructure can be facilitated and would be a useful link to develop other similar optoelectronic compounds in near future.

### Acknowledgement

One of the authors (YK Sharma) acknowledges the Council of Scientific & Industrial Research (CSIR) India for Senior Research Fellowship (grant no. 9/45(0842)2009) and USIC, Central instrument facility, University of Delhi, Delhi and IIT Roorkee.

### Reference

1. Srivastava, A.K.; Deepa, M.; Sood, K. N.; Erdem, E.; Eichel, R.-A. *Adv. Mat. Lett.* **2011**, *2*, 142.  
DOI: [10.5185/amlett.2011.1201](https://doi.org/10.5185/amlett.2011.1201)
2. Pan, Z. W.; Dai, Z. R.; Wang, Z. L. *Science* **2001**, *291*, 1947.  
DOI: [10.1126/science.1058120](https://doi.org/10.1126/science.1058120)
3. Trubelja, M. P.; Ryba, E.; Smith, D. K. *J. Mat. Sci.* **1996**, *31*, 1435.  
DOI: [10.1007/BF00357850](https://doi.org/10.1007/BF00357850)
4. Neurgaonkar, R. R.; Oliver, R.; Cory, W. K. *Ferroelectrics* **1994**, *160*, 265.  
DOI: [10.1080/00150199408222463](https://doi.org/10.1080/00150199408222463)
5. Clarke, R.; Siapkis, D. *J. Phys. C: Solid State Phys.* **1975**, *8*, 377.  
DOI: [10.1088/0022-3719/10/11/030](https://doi.org/10.1088/0022-3719/10/11/030)
6. Jamieson, P. B.; Abrahams, S. S.; Barnstein, J. L. *J. Chem. Phys.* **1968**, *48*, 5048.  
DOI: [10.1063/1.1668176](https://doi.org/10.1063/1.1668176)
7. Lenzo, P.V.; Spencer, E. G.; Ballman, A. A. *Appl. Phys. Lett.* **1967**, *11*, 23.  
DOI: [10.1063/1.1754944](https://doi.org/10.1063/1.1754944)
8. Abrahams, S. C.; Jamieson, P. B.; Bernstein, J. L. *J. Chem. Phys.* **1971**, *54*, 2355.  
DOI: [10.1063/1.1675186](https://doi.org/10.1063/1.1675186)
9. Neurgaonkar, R. K.; Corey, W. K. *J. Opt. Soc. Am. B* **1986**, *3*, 274.  
DOI: [10.1364/JOSAB.3.000274](https://doi.org/10.1364/JOSAB.3.000274)
10. Patro, P. K.; Deshmukh, R. D.; Kulkarni, A. R.; Harendranath, C. S. *J. Electroceram.* **2004**, *13*, 479.  
DOI: [10.1007/s10832-004-5145-4](https://doi.org/10.1007/s10832-004-5145-4)
11. Hornebecq, V.; Elissalde, C.; Porokhonsky, V.; Bovtun, V. Petzelt, J.; Gregora, I; Maglione, M.; Ravez, J. *J. Phys. Chem. Solids*, **2003**, *64*, 471.

- DOI: [10.1016/S0022-3697\(02\)00342-6](https://doi.org/10.1016/S0022-3697(02)00342-6)
12. Swartz, S. L.; Shrout, T. R.; Takenaka, T. *Am. Ceram. Soc. Bull.* **1997**, *76*, 51.  
DOI: [10.634540006723127.0030](https://doi.org/10.634540006723127.0030)
  13. Li, Y.; Zhao, J. P.; Wang, B. *Mater. Res. Bull.* **2004**, *39*, 365.  
DOI: [10.1016/j.materresbull.2003.11.002](https://doi.org/10.1016/j.materresbull.2003.11.002)
  14. Hirano, S.; Yogi, T.; Kikuta, K.; Ogiso, K. *J. Am. Ceram. Soc.* **1992**, *75*, 1697.  
DOI: [10.1111/j.1151-2916.1992.tb04251.x](https://doi.org/10.1111/j.1151-2916.1992.tb04251.x)
  15. Lu, S. G.; Mak, C. L.; Wong, K. H. *J. Am. Ceram. Soc.* **2001**, *84*, 79.  
DOI: [10.1063/1.1427419](https://doi.org/10.1063/1.1427419)
  16. Panda, A. B.; Pathak, A.; Pramanik, P. *Mater. Lett.* **2002**, *52*, 180.  
DOI: [10.1016/S0167-577X\(01\)00389-5](https://doi.org/10.1016/S0167-577X(01)00389-5)
  17. Glinchuk, M. D. *Brit. Ceram. Trans.* **2004**, *103*, 76.  
DOI: [10.1179/096797804225012792](https://doi.org/10.1179/096797804225012792)
  18. Bokov, A. A.; Ye, Z. G. *J. Mater. Sci.* **2006**, *41*, 31.  
DOI: [10.1007/s10853-005-5915-7](https://doi.org/10.1007/s10853-005-5915-7)
  19. Kleemann, W. *J. Mater. Sci.* **2006**, *41*, 129.  
DOI: [10.1007/s10853-005-5954-0](https://doi.org/10.1007/s10853-005-5954-0)
  20. Burns, G.; Dagol, F. H. *Ferroelectrics* **1990**, *104*, 25.  
DOI: [10.1080/00150199008223809](https://doi.org/10.1080/00150199008223809)
  21. Smolensky, G. A.; V. A. *Ispov. Dokl. Akad. Nauk. SSSR* **1954**, *9*, 653.
  22. Sakamoto, W. S.; Yogo, T.; Kikuta, K.; Ogiso, K.; Kawase, A.; Hirano, S. *J. Am. Ceram. Soc.* **1998**, *81*, 2692.  
DOI: [10.1111/j.1151-2916.1998.tb02678.x](https://doi.org/10.1111/j.1151-2916.1998.tb02678.x)
  23. Fang, T. T.; Wu, N.; Shiao, F. *J. Mat. Sci. Lett.* **1994**, *13*, 746.  
DOI: [10.1007/BF00776344](https://doi.org/10.1007/BF00776344)
  24. Nagata, K.; Yamamoto, Y.; Igarashi, H.; Okazaki, K. *Ferroelectrics* **1981**, *38*, 853.  
DOI: [10.1016/S0955-2219\(01\)00066-8](https://doi.org/10.1016/S0955-2219(01)00066-8)
  25. Patro, P. K.; Kulkarni, A. R.; Harendranath, C. S. *J. Euro. Ceram. Soc.* **2003**, *23*, 1329.  
DOI: [10.1016/S0955-2219\(02\)00293-5](https://doi.org/10.1016/S0955-2219(02)00293-5)
  26. Pasricha, R.; Ravi, V. *Mater. Chem. Phys.* **2005**, *94*, 34.  
DOI: [10.1016/j.matchemphys.2005.04.003](https://doi.org/10.1016/j.matchemphys.2005.04.003)
  27. Xu, Y.; Chen, J.; Xu, R.; Mackenzie, J. D. *Phys. Rev. B* **1991**, *44*, 35.  
DOI: [10.1103/PhysRevB.44.35](https://doi.org/10.1103/PhysRevB.44.35)
  28. Saxena, S.; Asokkumar, A. K.; Lal, B. *J. Sol-Gel Sci. Tech.* **2007**, *41*, 245.  
DOI: [10.1007/s10971-006-1503-9](https://doi.org/10.1007/s10971-006-1503-9)
  29. Patro, P. K.; Kulkarnia, A. R.; Gupta S. M.; Harendranath, C. S. *Physica B: Condensed Matter.* **2007**, *400*, 237.  
DOI: [10.1016/j.physb.2007.07.022](https://doi.org/10.1016/j.physb.2007.07.022)
  30. Hughes, S. W. *Phys. Educ.* **2006**, *41*, 445.  
DOI: [10.1088/0031-9120/41/5/011](https://doi.org/10.1088/0031-9120/41/5/011)
  31. Zhao, J.; Li, Y.; Wang, B.; Qing, L. *Ceram. Int.* **2004**, *30*, 613.  
DOI: [10.1016/j.ceramint.2003.07.007](https://doi.org/10.1016/j.ceramint.2003.07.007)
  32. Deshpande, S. B.; Potdar, H. S.; Godbole, P. D.; Date, S. K. *J. Am. Ceram. Soc.* **1992**, *75*, 2581.
  33. Kasprovicza, D.; Runkaa, T.; Majchrowskib, A.; Michalskib, E.; Drozdowska, M. *Physics Procedia*, **2009**, *2*, 539.  
DOI: [10.1016/j.phpro.2009.07.039](https://doi.org/10.1016/j.phpro.2009.07.039)
  34. Nishio, K.; Watanabe, Y.; Tsuchiya, T.; *26*, 245.  
DOI: [10.1023/a:1020707317411](https://doi.org/10.1023/a:1020707317411)
  35. Deneva, M.; *J. Univ. Chem. Tech. Metallurgy* **2010**, *45*, 358.
  36. B. D. Cullity, Elements of X-ray diffraction Addison-Wesley London **1978**, pp. 99.
  37. Ishikawa, K.; Yoshikawa, K.; Ukada, N. *Phys. Rev. B* **1988**, *37*, 5852.  
DOI: [10.1103/PhysRevB.37.5852](https://doi.org/10.1103/PhysRevB.37.5852)
  38. Ho, M. M. T.; Mark, C. L.; Wong, K. H. *J. Euro. Ceram. Soc.* **1998**, *19*, 1115.  
DOI: [10.1016/S0955-2219\(98\)00385-9](https://doi.org/10.1016/S0955-2219(98)00385-9)
  39. Kasprovicza, D.; Lapinski, A.; Runka, T.; Spgehini, A.; Bettinelli, M. *J. Alloys Comp.* **2009**, *478*, 30.  
DOI: [10.1016/j.jallcom.2008.11.096](https://doi.org/10.1016/j.jallcom.2008.11.096)
  40. Ross, S. D. *J. Phys. C.: Solid St. Phys.* **1970**, *3*, 1788.  
DOI: [10.1088/0022-3719/3/8/018](https://doi.org/10.1088/0022-3719/3/8/018)
  41. Xu, T.; Zhao, X.; Zhu, Y. *J. Phys. Chem. B* **2006**, *110*, 25825.  
DOI: [10.1021/jp065307k](https://doi.org/10.1021/jp065307k)
  42. Chen, W.; Kume, S.; Duran, C.; Watari, K. *J. Europ. Ceram. Soc.* **2006**, *26*, 647.  
DOI: [10.1016/j.jeurceramsoc.2005.06.010](https://doi.org/10.1016/j.jeurceramsoc.2005.06.010)
  43. Blasse, G.; VanLeur, M. G. *J. Mater. Res. Bull.* **1985**, *20*, 1037.  
DOI: [10.1016/0025-5408\(85\)90083-2](https://doi.org/10.1016/0025-5408(85)90083-2)
  44. Gao, M.; Pankrath, R.; Kapphan, S.; Vikhnin, V. *Appl. Phys. B: Lasers Opt.* **1999**, *B68*, 849.
  45. Srivastava, A. M.; Ackerman, J. F.; Beers, W. W. *J. Solid State Chem.* **1997**, *134*, 187.  
DOI: [10.1006/jssc.1997.7574](https://doi.org/10.1006/jssc.1997.7574)
  46. Wachtel, A. J. *Electrochem. Soc.* **1964**, *111*, 534.  
DOI: [10.1149/1.2426176](https://doi.org/10.1149/1.2426176)
  47. Zhang, W. F.; Yin, Z.; Zhang, M. S. *Appl. Phys. A* **2000**, *70*, 93.  
DOI: [10.1016/j.matlet.2003.07.025](https://doi.org/10.1016/j.matlet.2003.07.025)
  48. Romero, J. J.; Andreetta, M. R. B.; Andreetta, E. R. M.; Bausa, L. E.; Hernandez, A. C.; Sole, J. G. *Appl. Phys. A* **2004**, *78*, 1037.  
DOI: [10.1007/s00339-003-2151-3](https://doi.org/10.1007/s00339-003-2151-3)
  49. Ni, Y.; Wang, X.; Hong, J. *Mater. Res. Bull.* **2009**, *44*, 1797.
  50. Ngai, K. L.; Rendell, R. W. *Phys. Rev.* **2000**, *61*, 9393.  
DOI: [10.1103/PhysRevB.61.9393](https://doi.org/10.1103/PhysRevB.61.9393)
  51. Trubelja, M. P.; Raba, E.; Smith, D. K., *J. Mater. Sci.* **1996**, *31*, 1435.  
DOI: [10.1007/BF00357850](https://doi.org/10.1007/BF00357850)
  52. K. Chi Kao, Dielectric phenomena in Solids, Elsevier Academic Press (2004).
  53. Gupta, V.; Bamzai, K. K.; Kotru, P. N.; Wanklyn, B. M. *Mater. Sci. Eng. B* **2006**, *130*, 163.  
DOI: [10.1016/j.mseb.2006.03.006](https://doi.org/10.1016/j.mseb.2006.03.006)
  54. Huang, W. H.; Vichland, D.; Neurgaonkar, R. R. *J. Appl. Phys.* **1994**, *76*, 490.  
DOI: [10.1063/1.357100](https://doi.org/10.1063/1.357100)
  55. Kulkarni, R.; Patro, P. K.; Gupta, S. M.; Harendranath, C. S. IEEE International Symposium on Applications of Ferroelectrics, 17th, Santa Fe, NM, United States, Feb. 23-28, 23 (2008).  
DOI: [10.1109/ISAF.2008.4693890](https://doi.org/10.1109/ISAF.2008.4693890)

## Advanced Materials Letters

### Publish your article in this journal

ADVANCED MATERIALS Letters is an international journal published quarterly. The journal is intended to provide top-quality peer-reviewed research papers in the fascinating field of materials science particularly in the area of structure, synthesis and processing, characterization, advanced-state properties, and applications of materials. All articles are indexed on various databases including DOAJ and are available for download for free. The manuscript management system is completely electronic and has fast and fair peer-review process. The journal includes review articles, research articles, notes, letter to editor and short communications.

